Journal of Materials Chemistry A

PAPER

View Article Online
View Journal | View Issue

Cite this: J. Mater. Chem. A, 2019, 7, 9130

A 1.51 V pH neutral redox flow battery towards scalable energy storage†

Jian Luo, Wenda Wu, Camden Debruler, Bo Hu, Maowei Hu and T. Leo Liu *

Aqueous redox flow batteries using low-cost organic and inorganic active materials have received growing interest for sustainable energy storage. In this study, a low-cost, high redox potential (1.08 V *vs.* NHE) and high capacity ammonium bromide (NH_4Br, 214.4 A h L^{-1}) catholyte was coupled with an organic viologen anolyte to demonstrate 1.51 V high voltage $(SPr)_2V/Br^-$ aqueous redox flow batteries under pH neutral conditions for the first time. Benefitting from the high water solubility of both the NH_4Br catholyte and $(SPr)_2V$ anolyte, the newly designed $(SPr)_2V/Br^-$ organic flow battery was operated at up to 1.5 M and an energy density of up to 30.4 W h L^{-1}. Using multiwall carbon nanotubes as an electrochemical additive for the Br_3^-/Br^- redox couple, the highly energy dense $(SPr)_2V/Br^-$ flow battery manifested outstanding current performance, up to 78% energy efficiency at 40 mA cm^{-2} current density and 227 mW cm^{-2} power density, the highest power density known for pH neutral organic flow batteries.

Received 8th February 2019
Accepted 12th March 2019

DOI: 10.1039/c9ta01469a

rsc.li/materials-a

1. Introduction

To efficiently utilize renewable energy sources and achieve a sustainable society, advanced large-scale energy storage technologies are highly demanded.[1–3] Among various energy storage devices, aqueous redox flow batteries (ARFBs) have been recognized as a suitable technology for large-scale energy storage.[2,3] ARFBs have the advantages of independent power and energy control, excellent rate performance and power generation, and use of inexpensive and nonflammable electrolytes, and thus are well suited for the storage of intermittent and dispersed renewable energy (*e.g.*, wind and solar).[2,3] However, traditional vanadium redox flow batteries (VRFBs) encounter several critical barriers for broad energy storage applications, including scarce and pricy vanadium resources, side-reactions (*i.e.*, hydrogen and oxygen formation), vanadium species crossover, and hazardous and strongly acidic corrosive electrolytes.[2,3] To realize affordable and sustainable electrochemical energy storage, low-cost organic and inorganic redox active materials have received increasing attention for RFB studies in recent years.[4–25]

Bromides are redox active inorganic materials which widely exist in nature (*e.g.*, 65 mg L^{-1} in seawater, which is around 0.2% of all dissolved salts). Lots of bromide salts are highly soluble in water with a high redox potential $E_{1/2}(Br_3^-/Br^-)$ at 1.08 V (*vs.* NHE). Zn/Br^- RFBs have received massive interest and continuous effort has been made to commercialize them.[26] However, the current and power performance of Zn/Br^- RFBs is limited by the formation of Zn dendrites on the anode electrode.[26] In addition, power and energy are not fully decoupled in the hybrid Zn/Br^- systems because of the deposition/stripping of the solid state zinc electrode.[2,3] Meanwhile, to avoid the hydrolysis of the Zn^{2+} cation, the electrolytes need to be kept at acidic pH; however, zinc anode corrosion due to the H_2 evolution reaction is significant and leads to charge imbalance.[26] Other anode materials such as polysulfide (S_x^{2-}) and anthraquinone (AQ) derivatives were used to pair with the Br_3^-/Br^- redox couple for RFB application.[27–29] However, the crossover of sulfide limited the battery performance of S_x^{2-}/Br^- ARFBs,[3,27] some AQ derivatives were degraded in the presence of Br_2 through bromination reactions.[28] Moreover, AQ/Br^- ARFBs were demonstrated under strongly acidic corrosive conditions (usually 3.0 M HBr).[8,28] Thus, utilization of the low-cost, high redox potential bromide catholyte is highly desired in high performance benign pH neutral ARFBs, which remains unknown so far.

We and other groups have demonstrated that viologen molecules are highly stable tunable anolytes in aqueous organic redox flow batteries (AORFBs) under pH neutral conditions.[9,10,21,30–32] However, the low redox potential and low solubility of catholytes limited energy (less than 13.0 W h L^{-1}) and power (less than 130 mW cm^{-2}) densities of the related pH neutral AORFBs (Fig. 1). High voltage and energy density was obtained by using the N^{Me}-TEMPO catholyte; however, the cost of the redox material is fairly high.[30,31] Moreover, due to the relatively low ionic conductivity of pH neutral electrolytes, the power densities of the neutral AORFBs are still not competitive with those of strongly alkaline and acidic RFBs.[8,22] Herein, we exploit the high redox potential (1.08 V *vs.* NHE) and high

The Department of Chemistry and Biochemistry, Utah State University, Logan, Utah 84322, USA. E-mail: Leo.Liu@usu.edu

† Electronic supplementary information (ESI) available: Experimental procedures, post-cell NMR and CV analysis, cell impedance spectroscopy, and battery data. See DOI: 10.1039/c9ta01469a

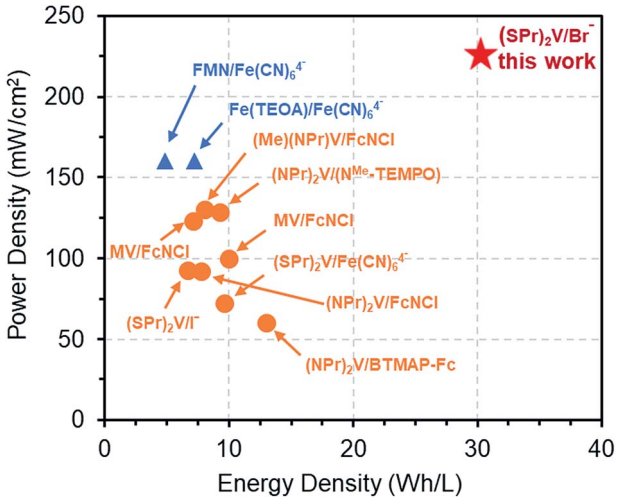

Fig. 1 Comparison of the demonstrated energy density and power density of the AORFB in this work and previously reported representative pH neutral (orange) and alkaline (blue) AORFBs. Neutral AORFBs: MV/FcNCl,[21,35] $(NPr)_2V$/FcNCl,[30] $(NPr)_2V/(N^{Me}$-TEMPO),[36] (Me) (NPr)V/FcNCl,[30] $(SPr)_2V/I^-$,[33] $(SPr)_2V/Fe(CN)_6^{4-}$,[34] and $(NPr)_2V$/BTMAP-Fc;[32] alkaline AORFBs: FMN/$Fe(CN)_6^{4-}$ (ref. 37) and Fe(TEOA)/$Fe(CN)_6^{4-}$.[38]

capacity (8.0 M or 214.4 A h L^{-1}) ammonium bromide catholyte, NH_4Br, in pH neutral AORFB for the first time by pairing with 1,1′-bis(3-sulfonatopropyl)-4,4′-bipyridinium ($(SPr)_2V$) as an anolyte.[33,34] With the high solubility of both $(SPr)_2V$[33,34] and NH_4Br and their large redox gap (1.51 V), a high operating energy density of 30.4 W h L^{-1} was achieved for the $(SPr)_2V/Br^-$ AORFB, among the most energy dense AORFBs. Using multiwall carbon nanotubes (MWCNTs) as an electrode additive to improve the electrochemical kinetics of the Br_3^-/Br^- redox couple, a 1.5 M $(SPr)_2V/Br^-$ AORFB was able to cycle at 40–100 mA cm^{-2} with an energy efficiency of up to 78% and a coulombic efficiency (CE) >98%. Notably, the 1.5 M $(SPr)_2V/Br^-$ AORFB delivered a power density of 227 mW cm^{-2} even under pH neutral conditions, which is the highest value known for the pH neutral AORFBs, and it is even higher than that of some strongly alkaline AORFBs (Fig. 1).[21,30,32–38] The low cost, and high energy and power densities of the $(SPr)_2V/Br^-$ AORFB makes it promising for scalable renewable energy storage.

2. Experimental procedures

Chemicals and manipulations

Chemicals were purchased from Sigma-Aldrich or TCI Chemicals, stored in an argon glovebox and used directly. $(SPr)_2V$ was synthesized and characterized as reported previously by us.[33,34] DI water was purged overnight using N_2 before use. All batteries were tested under a N_2 atmosphere; the pH values of electrolytes were adjusted to 7.0 using diluted HCl or $NH_3 \cdot H_2O$. Conductivities and pH values of the electrolytes were measured using a Mettler Toledo conductivity meter or a Mettler Toledo pH meter at room temperature. The ^{1}H-NMR spectrum was collected using a Bruker 500 MHz NMR spectrometer. All electrochemical experiments were conducted with a Gamry 1000E or 5000E potentiostat. Battery tests were performed using a Land battery testing system.

Cyclic voltammetry studies

A Gamry 1000E potentiostat was used to perform the CV tests with a three-electrode system in a 0.5 M NH_4Cl electrolyte solution under a N_2 atmosphere. A PEEK-encased 3 mm diameter glassy carbon or Pt disk was used as the working electrode. A glassy carbon rod was used as the counter electrode. An Ag/AgCl reference electrode was constructed by submerging a silver wire in 3.0 M KCl solution. Before each test, the working electrode was polished with 0.05 micron alumina powder and rinsed with DI water. Potential values were corrected to NHE using a (ferrocenylmethyl)trimethylammonium chloride (FcNCl) internal standard with a known redox potential at 0.61 V *vs.* NHE. The scan rate for all the CV tests in this study was 100 mV s^{-1}.

Half-cell flow battery tests

The half-cell flow battery for the $(SPr)_2V/(SPr)_2V^{-\bullet}$ redox couple was constructed with two carbon electrolyte chambers, two graphite felt electrodes (SGL Carbon Group, Germany), a piece of cation-exchange membrane (Nafion® 212 membrane) as the separator sandwiched between graphite felts, and two copper plates as current collectors. Each carbon chamber was connected with an electrolyte reservoir using a piece of Viton tubing. The electrolyte reservoir is homemade and is a 10 mL glass tube (2 cm inner diameter). The effective area of the cell was 10 cm^2. The circulation of the electrolytes was implemented using a Masterflex L/S peristaltic pump (Cole-Parmer, Vernon Hills, IL) at a flow rate of 60 mL min^{-1}. Each reservoir contains 12 mL of 1.0 M NH_4Cl electrolyte containing 0.5 M active materials. Before cell cycling, nitrogen flow was used to purge the reservoirs to remove O_2. The flow cell was charged/discharged galvanostatically at room temperature on a Land battery tester in the voltage window of −0.25 to 0.25 V at current densities of 40, 60, 80, and 100 mA cm^{-2}. Post cell analysis of the electrolytes after full discharge was conducted by using ^{1}H-NMR and CV at the end of 500 cycles.

Full-cell flow battery tests

The setup of the $(SPr)_2V/Br$ AORFBs is the same as the $(SPr)_2V/(SPr)_2V^{-\bullet}$ half-cell battery. For the 0.1 M RFB: 12.0 mL of 0.1 M $(SPr)_2V$ in 1.0 M NH_4Br solution was used as an anolyte, 0.1 M Br_2 in 1.2 M NH_4Br solution was used as a catholyte, a piece of Nafion® 212 membrane was used as a separator. For the 1.0 M RFB: 12.0 mL of 1.0 M $(SPr)_2V$ in 1.5 M NH_4Br solution was used as an anolyte, 0.2 M Br_2 in 3.5 M NH_4Br solution was used as a catholyte, a piece of Nafion® 115 membrane was used as a separator. For the 1.5 M RFB: 12.0 mL of 1.5 M $(SPr)_2V$ in 1.0 M NH_4Br solution was used as an anolyte, 0.2 M Br_2 in 4.0 M NH_4Br solution was used as a catholyte, a piece of Nafion® 115 membrane was used as a separator. The cell was galvanostatically charged to 1.7 or 1.8 V and discharged to 0.1 V at current densities ranging from 40 to 100 mA cm^{-2}.

Preparation of the MWCNT-modified Glassy Carbon Electrode (GCE)

The multiwall carbon nanotube (MWCNT)-modified GCE was prepared as reported in the literature.[39] In brief, 2.5 mg of MWCNTs were dispersed in 750 μL of a deionized water and isopropanol (1 : 5 ratio) mixture by ultra-sonication. Thirty microliters of MWCNT slurry was dropped onto the polished GCE and dried under ambient conditions for 30 min to evaporate the solvent completely.

Preparation of MWCNT-loaded graphite felt (MWCNT@GF) electrodes

The MWCNT@GF electrode was prepared using a similar procedure to that previously reported.[39] Typically, a graphite felt electrode (SGL Carbon Group, Germany) (10 cm^2) was subjected to ultra-sonication in deionized water and dried at 60 °C for 5 h. MWCNTs and DMF in a 1 : 1 weight and volume ratio were mixed together by ultra-sonication for about 10 min. The pre-treated GF was immersed in MWCNT–DMF solution and subjected to ultra-sonication for 2 hours. The MWCNT-loaded GF was dried at 100 °C for 24 h and weight changes indicated a loading of 0.8 mg cm^{-2}.

3. Results and discussion

Among common bromide salts (NH_4Br, NaBr, and KBr), ammonium bromide displayed high solubility/charge capacity and its aqueous solution also has high molar conductivity. In addition, the ammonium cation (NH_4^+) has a charge mobility comparable with K^+ but faster than Na^+ through a cation exchange membrane.[34] These advantageous physical properties highlight that NH_4Br is an optimal choice of redox active bromide catholyte for pH neutral AORFBs. The cyclic voltammogram of NH_4Br in 0.5 M NH_4Cl water solutions displays a reversible oxidation wave at 1.08 V *vs.* NHE (Scheme 1 and Fig. 2A), the combination of NH_4Br with $(SPr)_2V$ (−0.43 V *vs.* NHE) gives a battery voltage of 1.51 V, which is bracketed within the electrochemical window of water (HER at −1.43 and OER at 1.30 V, Fig. S1†). In addition, the electrochemical and chemical stability of the $(SPr)_2V$ anolyte in NH_4Cl was studied in a symmetric half-cell RFB using $(SPr)_2V$ and $(SPr)_2V^{-\bullet}$ in the anode and the cathode side, respectively. As shown in Fig. S2,† a 0.5 M $(SPr)_2V/(SPr)_2V^{-\bullet}$ half-cell RFB was tested using cut-off voltages of −0.25 and 0.25 V in a current density range of 40–100 mA cm^{-2}. At each current density, the half-cell battery delivered stable charge/discharge profiles and nearly 100% CE. To confirm the long-term durability of the $(SPr)_2V/(SPr)_2V^{-\bullet}$ couple, 500 cycle data were collected at 60 mA cm^{-2} using the half-cell battery. No capacity fading was observed during the battery cycling which indicated the excellent chemical stability of the $(SPr)_2V/(SPr)_2V^{-\bullet}$ redox couple. It was further confirmed by CV and ^{1}H-NMR post cycling analysis (Fig. S3 and S4†).

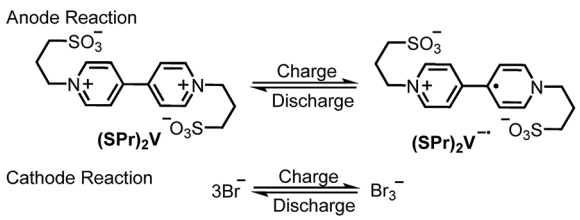

Scheme 1 The scheme of anode and cathode half-cell reactions for the $(SPr)_2V/Br^-$ AORFB.

The $(SPr)_2V/Br^-$ full-cell AORFB was first demonstrated using 0.1 M $(SPr)_2V$ in 1.0 M NH_4Br aqueous solution as the anolyte and 0.1 M Br_2 in 1.2 M NH_4Br aqueous solution as the catholyte, and a Nafion 212 cation-exchange membrane as the separator for NH_4^+ cation exchange. Herein, we chose NH_4^+ as the charge carrier for battery charge/discharge, due to its higher ionic conductivity than Na^+ and K^+ in the Nafion 212 cation-exchange membrane (Fig. S5†). Fig. 2 displays the performance of the 0.1 M $(SPr)_2V/Br^-$ AORFB. The flow battery was first evaluated at four current densities of 10, 20, 30, and 40 mA cm^{-2} within the charge/discharge voltage window between 0.1 and 1.7 V. At each current density, the battery delivered up to 97% capacity utilization at 10 mA cm^{-2} current density and >98% CE (Fig. 2B and D). Meanwhile, satisfactory VE and EE were obtained, *i.e.*, 83% VE and EE at 10 mA cm^{-2}. They retained 57% when the current was augmented to 40 mA cm^{-2} (Fig. 2D). The cycling stability of the 0.1 M $(SPr)_2V/Br^-$ AORFB was measured at 20 mA cm^{-2}. 7.1% capacity fading was observed after 100 charge/discharge cycles (30 hours), giving a capacity stability of 99.93% for each cycle or 99.76% for each hour (Fig. 2E). The average CE of the AORFB is 98.88%, slightly lower than 100% due to the crossover of Br_2 from the cathode side to the anode side.

To mitigate the crossover of Br_2 in the $(SPr)_2V/Br^-$ AORFBs, a thicker Nafion 115 cation-exchange membrane was used as a separator. And the $(SPr)_2V$ concentration was increased to 1.0 M. As shown in Fig. 2G, 1.0 M $(SPr)_2V$ in 1.5 M NH_4Br was used as the anolyte, 0.2 M Br_2 in 3.5 M NH_4Br was used as the catholyte, and the AORFB was charge/discharged between 1.7 V and 0.1 V at 40 mA cm^{-2} current density for 50 cycles without observing capacity decay (75 hours, 100% retention for each cycle or 100% retention for each hour). The AORFB delivered impressive electrochemical performance, including 80% EE, 81% VE, and 99.12% CE, on average. ^{1}H-NMR measurements were conducted on the anolyte after full discharge of the battery. As shown in Fig. S6,† the ^{1}H-NMR spectrum of the $(SPr)_2V$ remained unchanged after 50 charge/discharge cycles, which indicates no chemical degradation of $(SPr)_2V$ under the battery conditions. Polarization studies of the 0.1 and 1.0 M $(SPr)_2V/Br^-$ AORFBs were conducted at 100% and 50% SOC. As shown in Fig. 2F, a significant improvement of power density was observed when the electrolyte concentration increased from 0.1 M to 1.0 M (121.4 mW cm^{-2} at 100% SOC and 85.6 mW cm^{-2} at 50% SOC for the 1.0 M AORFB, and 82.0 mW cm^{-2} at 100% SOC and 71.6 mW cm^{-2} at 50% SOC for the 0.1 M AORFB). Meanwhile, the open circuit voltage (OCV) of both batteries was 1.57 V at 100% SOC.

To further boost the energy density of the $(SPr)_2V/Br^-$ AORFB, the concentration of the $(SPr)_2V$ anolyte was further increased to 1.5 M (30.35 W h L^{-1} operating energy density). However, due to the poor electrochemical kinetics of the Br_3^-/

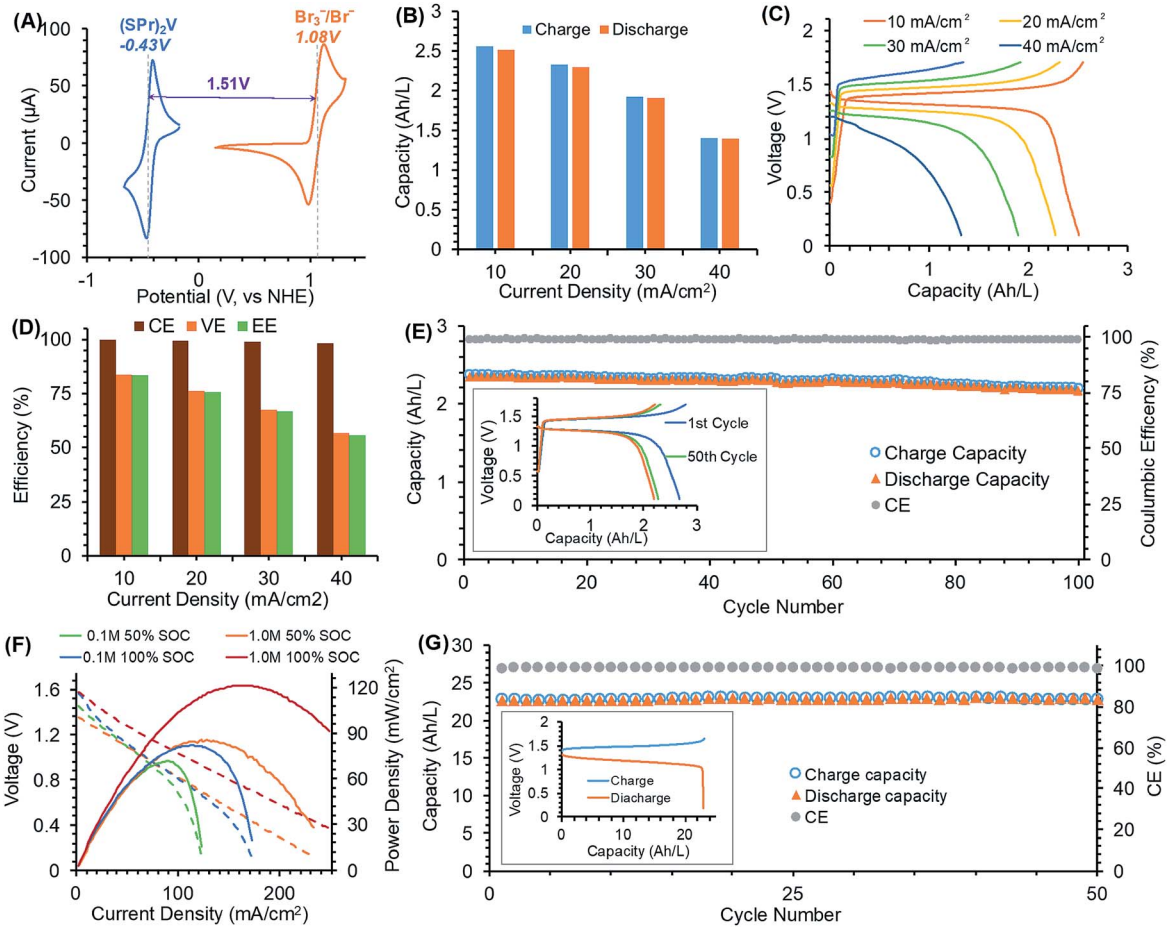

Fig. 2 (A) Cyclic voltammogram curves of 50 mM NH_4Br (1.08 V) or 4.0 mM $(SPr)_2V$ (−0.43 V) in 0.5 M NH_4Cl water solution (glassy carbon working electrode for $(SPr)_2V$ and Pt working electrode for NH_4Br). (B) Averaged charge and discharge capacities of the 0.1 M $(SPr)_2V/Br^-$ AORFB at different current densities (5 data points were collected at each current density). (C) Capacity–voltage plots of the 0.1 M $(SPr)_2V/Br^-$ AORFB at four current densities as labelled. (D) Battery efficiencies (CE, EE, and VE) of the AORFB at each operating current density. (E) Charge/discharge capacity and CE of the 0.1 M AORFB for 100 cycles (20 mA cm^{-2}). Testing conditions: 0.1 M $(SPr)_2V$ in 1.0 M NH_4Br and 1.2 M NH_4Br with 0.1 M Br_2; Nafion 212; pH 7.0. (F) Power density (solid) and polarization (dash) plots of 0.1 M and 1.0 M $(SPr)_2V/Br^-$ AORFBs at 100% and 50% SOC. (G) Charge/discharge capacity and CE of the 1.0 M AORFB for 50 cycles (40 mA cm^{-2}). Inset: charge and discharge curves of the AORFB. Testing conditions: 1.0 M $(SPr)_2V$ in 1.5 M NH_4Br and 3.5 M NH_4Br with 0.2 M Br_2; Nafion 115; pH 7.0.

Br^- redox couple on the carbon electrode and the low conductivity of the highly concentrated $(SPr)_2V$ solution (31.0 mS cm^{-1} conductivity of 1.5 M $(SPr)_2V$ in 1.0 M NH_4Br), the corresponding AORFB delivered high charge/discharge over-potential and poor efficiencies (Fig. S7†). Carbon nanotubes (CNTs) have been reported to facilitate the Br_3^-/Br^- redox couple.[39,40] Herein, multiwall carbon nanotubes (MWCNTs) were loaded as an efficient electrode additive into the cathode side graphite felt electrode to promote the energy efficiency and power density of the battery. The activity of MWCNTs to enhance the Br_3^-/Br^- redox couple was first investigated by CV measurements. As shown in Fig. 3A, the electrochemical reversibility and kinetics of the Br_3^-/Br^- redox couple were significantly improved by the MWCNT modification of the glassy carbon electrode, specifically, the peak–peak separation was reduced from 470 mV to 234 mV and the oxidative and reductive peak current ratio (I_{pO}/I_{pR}) was reduced from 2.1 to 0.83 (it is more near to 1.0). The MWCNT loaded graphite felt (MWCNT@GF) was used as cathode electrode for the 1.5 M $(SPr)_2V/Br^-$ AORFB. As shown in Fig. 3B, the AORFB displayed excellent current rate performance, only a 3.7% capacity decrease was observed with the current density increase from 40 mA cm^{-2} to 100 mA cm^{-2}. Meanwhile, the battery delivered high efficiencies, specifically, 79% VE and EE at 40 mA cm^{-2}, and they still retained 61% when the operating current density was increased to 100 mA cm^{-2} (Fig. 3C). The cycling stability of the 1.5 M $(SPr)_2V/Br^-$ battery was tested using 80 mA cm^{-2} for 30 cycles. The highly energy dense AORFB is fairly stable, 99.90% retention for each cycle or 99.89% retention for each hour with 99.5% average coulombic efficiency observed (Fig. S8†).

The performance of the 1.5 M $(SPr)_2V/Br^-$ AORFB was significantly improved by using the MWCNT additive in the cathode electrode. As displayed in Fig. 3D, charge and discharge over-potentials of the $(SPr)_2V/Br^-$ flow battery using the MWCNT@GF electrode were reduced by around 171 mV and 141 mV, respectively. In the same current range, the $(SPr)_2V/Br^-$

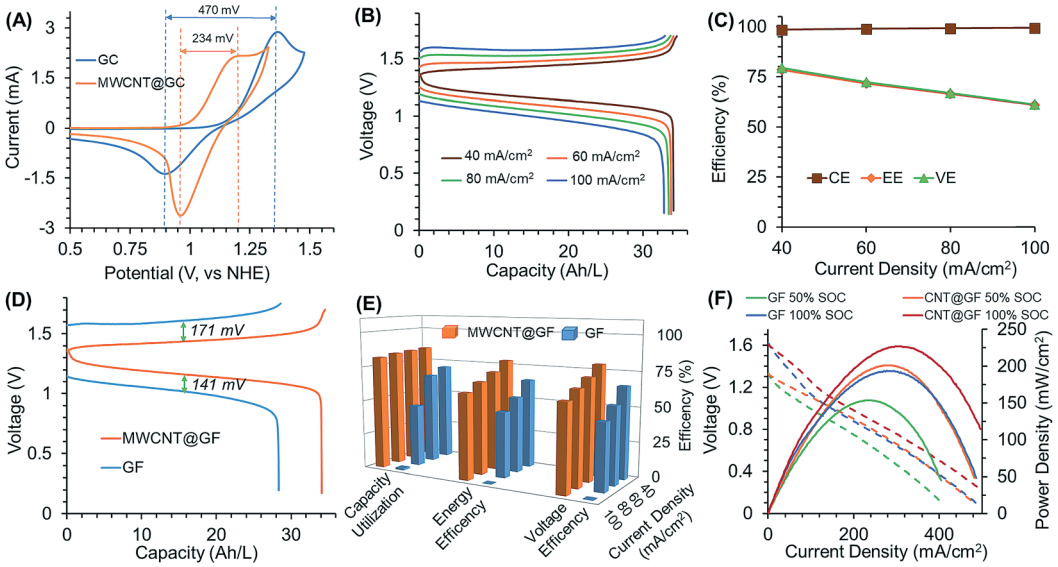

Fig. 3 (A) Cyclic voltammograms of 50 mM NH_4Br in 0.5 M NH_4Cl on a glassy carbon (GC) working electrode (blue) and MWCNT modified GC working electrode (orange). (B) Capacity–voltage plots of the 1.5 M $(SPr)_2V/Br^-$ AORFB at four current densities. (C) Battery efficiencies of the AORFB at each current density. (D) Charge/discharge curves of the 1.5 M $(SPr)_2V/Br^-$ AORFBs using MWCNT@GF (orange) and bare GF (blue) as the cathode at 40 mA cm^{-2}. (E) Capacity utilization and battery efficiency comparison of the 1.5 M $(SPr)_2V/Br^-$ AORFBs using MWCNT@GF (orange) and bare GF (blue) as the cathode at various current densities. (F) Power density (solid) and polarization (dash) plots at 100% and 50% SOC of the 1.5 M $(SPr)_2V/Br^-$ AORFBs using MWCNT@GF and bare GF as the cathode. Testing conditions: 1.5 M $(SPr)_2V$ in 1.0 M NH_4Br and 4.0 M NH_4Br with 0.2 M Br_2; Nafion 115; pH 7.0.

AORFB with the MWCNT@GF electrode displayed much better efficiencies than the one using the unmodified GF electrode (Fig. 3E). For example, the $(SPr)_2V/Br^-$ AORFB with MWCNT@GF delivered 84.8% capacity utilization, 79% VE, and 78% EE at 40 mA cm^{-2} (Fig. 3E, orange plot), much higher than those (70% capacity utilization, 65% EE, and 65% VE) of the AORFB using the unmodified GF electrode (Fig. 3E, blue plot, also Fig. S7†). In addition, the battery with the MWCNT@GF cathode electrode delivered much higher power densities than the one using the unmodified GF cathode electrode, for example, 227 mW cm^{-2} and 201 mW cm^{-2} power densities at 100% and 50% SOC, respectively, for the one using the MWCNT@GF cathode electrode; 198 mW cm^{-2} and 162 mW cm^{-2} power densities at 100% and 50% SOC, respectively, for the one using the unmodified GF cathode electrode. EIS measurements were conducted for an in-depth understanding of the activation mechanism of Br_3^-/Br^- by MWCNTs. As shown in Fig. S9,† the charge transfer resistance of the battery was decreased from 33 Ω cm^2 to 14 Ω cm^2 by using the MWCNT additive. It can be explained that MWCNTs with high surface areas can supply more active sites for the Br_3^-/Br^- redox reaction that induces improved electrochemical kinetics to minimize electrochemical polarization.[39]

As above mentioned, the bromide catholyte materials have several advantages, such as abundance, low-cost, and high redox potential. However, the fabrication of the Br_2-based RFB is still very challenging. On the one hand, Br_2 is highly corrosive and volatile. The volatilization of hazardous Br_2 will induce imbalance of matter and charge that affects the cycling performance of the RFB. And there are also environmental and health concerns. On the other hand, there is a chemical equilibrium between the Br_3^- anion and neutral Br_2 in the aqueous solution. The small neutral Br_2 molecules could easily crossover through the separator to react with the anolyte that will induce CE loss and irreversible capacity fading.[41] Some solutions have been reported to address these issues. For example, to solve the Br_2 volatilization issue, complexing reagents such as quaternary ammonium bromides can be used to trap the Br_3^- anion, then the liquid Br_2 volume and its vapor pressure can be minimized.[42–44] The addition of complexing reagents can also slow down the crossover of the Br_2 species. Additionally, advanced cation-exchange membranes to suppress the bromine crossover are highly demanded for Br-based ARFBs.[45] Besides these two options, bipolar electrolytes and symmetric battery design can also be considered. It is clear that there is a wide design space to further improve the electrochemical performance of the $(SPr)_2V/Br^-$ AORFB. For instance, an ongoing effort in our lab is to identify complexing agents to stabilize the Br_3^-/Br^- catholyte.

4. Conclusion

In summary, a low-cost, high potential ammonium bromide catholyte was applied in the pH neutral AORFB for the first time. A 1.51 V pH neutral $(SPr)_2V/Br^-$ AORFB was demonstrated at a high concentration of 1.5 M with an energy density of 30.35 W h L^{-1}. Using the MWCNT electrode additive for the Br_3^-/Br^- redox couple, the 1.5 M $(SPr)_2V/Br^-$ AORFB delivered up to 78% EE and 227 mW cm^{-2} power density at 100% SOC, which is the highest power density value ever reported for pH neutral AORFBs. The low cost, high energy and power densities of the

viologen/Br^- flow battery reported in this work make it a viable candidate for economical and sustainable storage of renewable energy.

5. Author contributions

T. L. L. designed the project. J. L. conducted experiments. W. W. helped in collecting and analyzing the battery data. T. L. L. and J. L. analyzed experimental data and prepared the manuscript, and all authors contributed to revising the manuscript.

6. Declaration of interests

A patent application was submitted based on the results reported herein.

Conflicts of interest

A patent application was submitted based on the results reported herein.

Acknowledgements

We acknowledge the financial support for this research from the National Science Foundation Career Award (grant no. 1847674), faculty startup funds from Utah State University and the Utah Science Technology and Research initiative (USTAR) UTAG award. C. D. is grateful for the USU Presidential Doctoral Research Fellowship provided by USU. B. H. is grateful for the China CSC Abroad Studying Fellowship and the Utah Energy Triangle Student Award provided by the Office of Energy of the Utah State government to support his graduate program. M. H. is grateful for the China CSC Abroad Studying Fellowship provided to support her graduate program.

References

1 B. Dunn, H. Kamath and J.-M. Tarascon, *Science*, 2011, **334**, 928–935.
2 Z. Yang, J. Zhang, M. C. W. Kintner-Meyer, X. Lu, D. Choi, J. P. Lemmon and J. Liu, *Chem. Rev.*, 2011, **111**, 3577–3613.
3 G. L. Soloveichik, *Chem. Rev.*, 2015, **115**, 11533–11558.
4 J. Winsberg, T. Hagemann, T. Janoschka, M. D. Hager and U. S. Schubert, *Angew. Chem., Int. Ed.*, 2017, **56**, 686–711.
5 P. Leung, A. A. Shah, L. Sanz, C. Flox, J. R. Morante, Q. Xu, M. R. Mohamed, C. Ponce de León and F. C. Walsh, *J. Power Sources*, 2017, **360**, 243–283.
6 X. Wei, W. Pan, W. Duan, A. Hollas, Z. Yang, B. Li, Z. Nie, J. Liu, D. Reed, W. Wang and V. Sprenkle, *ACS Energy Lett.*, 2017, **2**, 2187–2204.
7 Y. Ding, C. Zhang, L. Zhang, Y. Zhou and G. Yu, *Chem. Soc. Rev.*, 2018, **47**, 69–103.
8 B. Huskinson, M. P. Marshak, C. Suh, S. Er, M. R. Gerhardt, C. J. Galvin, X. Chen, A. Aspuru-Guzik, R. G. Gordon and M. J. Aziz, *Nature*, 2014, **505**, 195.
9 T. Janoschka, N. Martin, U. Martin, C. Friebe, S. Morgenstern, H. Hiller, M. D. Hager and U. S. Schubert, *Nature*, 2015, **527**, 78.
10 T. Liu, X. Wei, Z. Nie, V. Sprenkle and W. Wang, *Adv. Energy Mater.*, 2016, **6**, 1501449.
11 J. D. Milshtein, A. P. Kaur, M. D. Casselman, J. A. Kowalski, S. Modekrutti, P. L. Zhang, N. Harsha Attanayake, C. F. Elliott, S. R. Parkin, C. Risko, F. R. Brushett and S. A. Odom, *Energy Environ. Sci.*, 2016, **9**, 3531–3543.
12 L. Zhang, C. Zhang, Y. Ding, K. Ramirez-Meyers and G. Yu, *Joule*, 2017, **1**, 623–633.
13 C. S. Sevov, D. P. Hickey, M. E. Cook, S. G. Robinson, S. Barnett, S. D. Minteer, M. S. Sigman and M. S. Sanford, *J. Am. Chem. Soc.*, 2017, **139**, 2924–2927.
14 A. Hollas, X. Wei, V. Murugesan, Z. Nie, B. Li, D. Reed, J. Liu, V. Sprenkle and W. Wang, *Nat. Energy*, 2018, **3**, 508–514.
15 M. Zhou, Q. Huang, T. N. Pham Truong, J. Ghilane, Y. G. Zhu, C. Jia, R. Yan, L. Fan, H. Randriamahazaka and Q. Wang, *Chem*, 2017, **3**, 1036–1049.
16 C. Yang, G. Nikiforidis, J. Y. Park, J. Choi, Y. Luo, L. Zhang, S.-C. Wang, Y.-T. Chan, J. Lim, Z. Hou, M.-H. Baik, Y. Lee and H. R. Byon, *Adv. Energy Mater.*, 2018, **8**, 1702897.
17 M. Burgess, K. Hernández-Burgos, J. K. Schuh, J. Davila, E. C. Montoto, R. H. Ewoldt and J. Rodríguez-López, *J. Am. Chem. Soc.*, 2018, **140**, 2093–2104.
18 W. Li, H.-C. Fu, Y. Zhao, J.-H. He and S. Jin, *Chem*, 2018, **4**, 2644–2657.
19 J. Huang, L. Cheng, R. S. Assary, P. Wang, Z. Xue, A. K. Burrell, L. A. Curtiss and L. Zhang, *Adv. Energy Mater.*, 2015, **5**, 1401782.
20 J. Huang, Z. Yang, V. Murugesan, E. Walter, A. Hollas, B. Pan, R. S. Assary, I. A. Shkrob, X. Wei and Z. Zhang, *ACS Energy Lett.*, 2018, **3**, 2533–2538.
21 B. Hu, C. DeBruler, Z. Rhodes and T. L. Liu, *J. Am. Chem. Soc.*, 2017, **139**, 1207–1214.
22 K. Lin, Q. Chen, M. R. Gerhardt, L. Tong, S. B. Kim, L. Eisenach, A. W. Valle, D. Hardee, R. G. Gordon, M. J. Aziz and M. P. Marshak, *Science*, 2015, **349**, 1529–1532.
23 Y. Ding, C. Zhang, L. Zhang, H. Wei, Y. Li and G. Yu, *ACS Energy Lett.*, 2018, **3**, 2641–2648.
24 C. Zhang, Z. Niu, Y. Ding, L. Zhang, Y. Zhou, X. Guo, X. Zhang, Y. Zhao and G. Yu, *Chem*, 2018, **4**, 2814–2825.
25 C. Zhang, L. Zhang, Y. Ding, S. Peng, X. Guo, Y. Zhao, G. He and G. Yu, *Energy Storage Materials*, 2018, **15**, 324–350.
26 A. Khor, P. Leung, M. R. Mohamed, C. Flox, Q. Xu, L. An, R. G. A. Wills, J. R. Morante and A. A. Shah, *Materials Today Energy*, 2018, **8**, 80–108.
27 C. Ponce de León, A. Frías-Ferrer, J. González-García, D. A. Szánto and F. C. Walsh, *J. Power Sources*, 2006, **160**, 716–732.
28 M. R. Gerhardt, L. Tong, R. Gómez-Bombarelli, Q. Chen, M. P. Marshak, C. J. Galvin, A. Aspuru-Guzik, R. G. Gordon and M. J. Aziz, *Adv. Energy Mater.*, 2017, **7**, 1601488.
29 R. J. Remick and P. G. P. Ang, *U.S. Pat.*, 4485154, 1984.
30 C. DeBruler, B. Hu, J. Moss, X. Liu, J. Luo, Y. Sun and T. L. Liu, *Chem*, 2017, **3**, 961–978.

31 T. Janoschka, N. Martin, M. D. Hager and U. S. Schubert, *Angew. Chem., Int. Ed.*, 2016, **55**, 14427–14430.
32 E. S. Beh, D. De Porcellinis, R. L. Gracia, K. T. Xia, R. G. Gordon and M. J. Aziz, *ACS Energy Lett.*, 2017, **2**, 639–644.
33 C. DeBruler, B. Hu, J. Moss, J. Luo and T. L. Liu, *ACS Energy Lett.*, 2018, **3**, 663–668.
34 J. Luo, B. Hu, C. Debruler, Y. Bi, Y. Zhao, B. Yuan, M. Hu, W. Wu and T. L. Liu, *Joule*, 2019, **3**, 149–163.
35 B. Hu, C. Seefeldt, C. DeBruler and T. L. Liu, *J. Mater. Chem. A*, 2017, **5**, 22137–22145.
36 B. Hu, Y. Tang, J. Luo, G. Grove, Y. Guo and T. L. Liu, *Chem. Commun.*, 2018, **54**, 6871–6874.
37 A. Orita, M. G. Verde, M. Sakai and Y. S. Meng, *Nat. Commun.*, 2016, **7**, 13230.
38 K. Gong, F. Xu, J. B. Grunewald, X. Ma, Y. Zhao, S. Gu and Y. Yan, *ACS Energy Lett.*, 2016, **1**, 89–93.
39 Y. Munaiah, S. Suresh, S. Dheenadayalan, V. K. Pillai and P. Ragupathy, *J. Phys. Chem. C*, 2014, **118**, 14795–14804.
40 Y. Munaiah, S. Dheenadayalan, P. Ragupathy and V. K. Pillai, *ECS J. Solid State Sci. Technol.*, 2013, **2**, M3182–M3186.
41 G. Li, Y. Jia, S. Zhang, X. Li, J. Li and L. Li, *J. Appl. Electrochem.*, 2017, **47**, 261–272.
42 Q. Lai, H. Zhang, X. Li, L. Zhang and Y. Cheng, *J. Power Sources*, 2013, **235**, 1–4.
43 D. J. Eustace, *J. Electrochem. Soc.*, 1980, **127**, 528–532.
44 J.-D. Jeon, H. S. Yang, J. Shim, H. S. Kim and J. H. Yang, *Electrochim. Acta*, 2014, **127**, 397–402.
45 B. Huskinson, M. P. Marshak, M. R. Gerhardt and M. J. Aziz, *ECS Trans.*, 2014, **61**, 27–30.